Supplement of Atmos. Chem. Phys., 17, 297–311, 2017
http://www.atmos-chem-phys.net/17/297/2017/
doi:10.5194/acp-17-297-2017-supplement

Atmospheric Chemistry and Physics Open Access EGU

Supplement of

Particle settling and vertical mixing in the Saharan Air Layer as seen from an integrated model, lidar, and in situ perspective

Josef Gasteiger et al.

Correspondence to: Josef Gasteiger (josef.gasteiger@univie.ac.at)

S-1 Temporal evolution of size distribution in H2

We assume a diurnal cycle of the convection activity in H2. Thus, each night a fraction of the particles is removed from the SAL due to settling (Eq. 5). As a consequence, at the beginning of each night only a fraction of the initially available particles is present in the SAL, which is illustrated in Fig. 3 for ξ_{vc}=0.90. Fig. S-1 shows its effect on the number, area, and volume distribution, resulting from the multiplication of the fraction shown in Fig. 3 with the initial distribution. The different colors denote different i_{night} (same colors as in Fig. 3). The blue lines represent the initial size distribution.

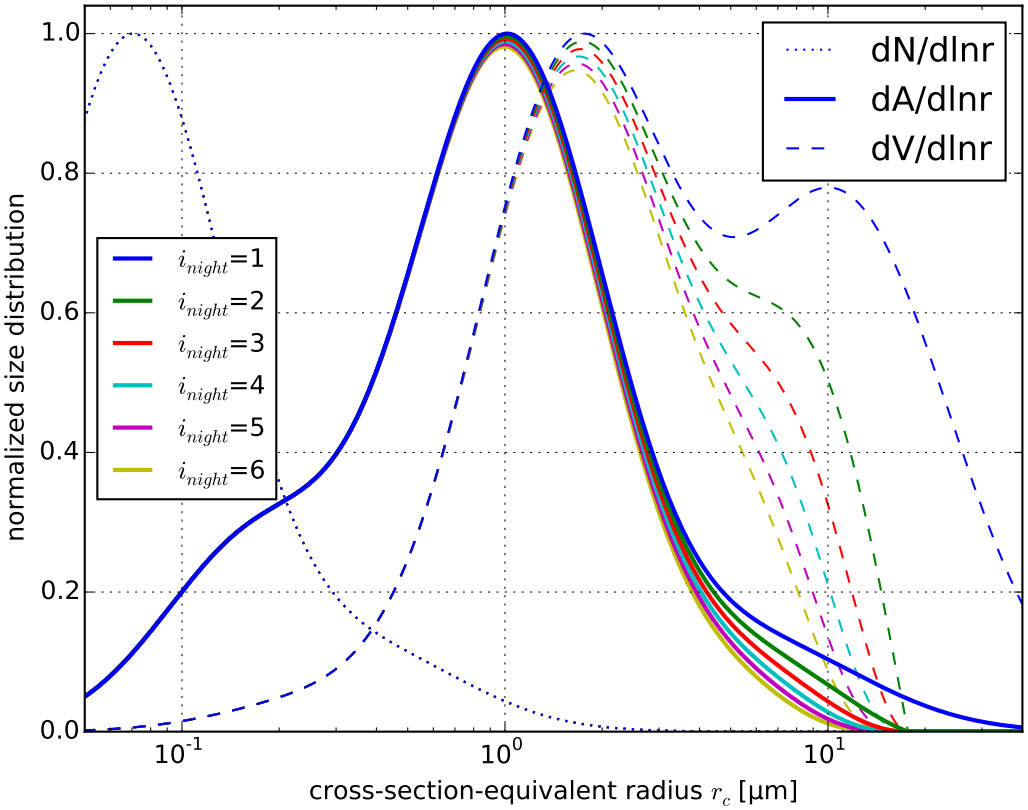

Figure S-1: Normalized number, area, and volume size distribution of mineral fraction (without WASO) at the beginning of each night for ξ_{vc}=0.90 and [H2, i_{night}, 0 h]. Colors denote different i_{night} (same colors as in Fig. 3)

The following table shows the effective radius $r_{\mathrm{eff}} = \frac{\int r^3 n(r) dr}{\int r^2 n(r) dr}$ of the size distributions at the beginning of each night ([H2, i_{night}, 0 h]):

i_{night}	1	2	3	4	5	6
r_{eff} with WASO	1.24 μm	0.99 μm	0.92 μm	0.88 μm	0.85 μm	0.82 μm
r_{eff} without WASO	1.73 μm	1.38 μm	1.29 μm	1.23 μm	1.19 μm	1.15 μm

S-2 Back-trajectories for case study 11 July 2013

In Section 4.1 we compare our model results with lidar measurements from around 0 UTC on 11 July 2013. We assume that the measured SAL aerosol left the African continent about 5 days before. This estimation is based on back-trajectory analyses using HYSPLIT as shown in Fig. S-2.

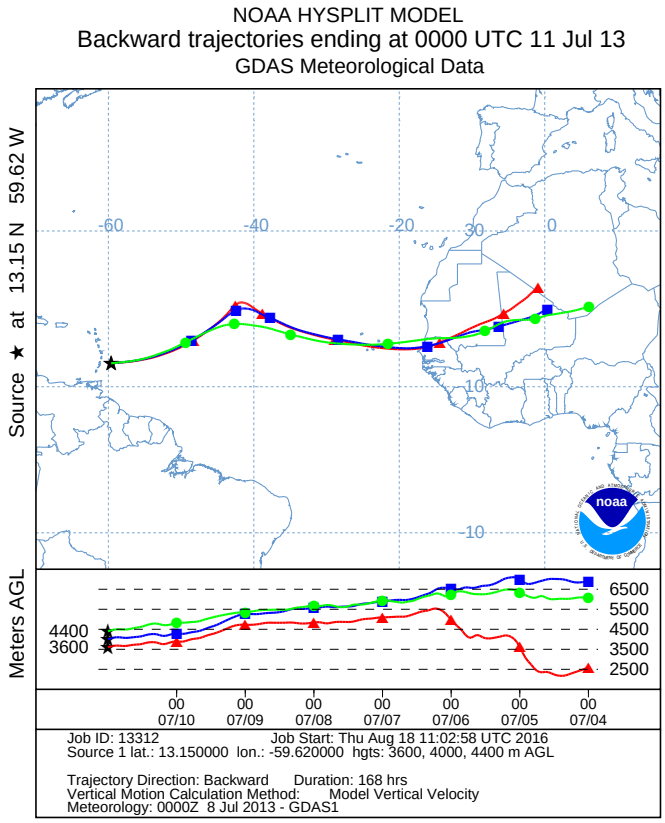

Figure S-2: Back-trajectories for SAL layer over Barbados at 0 UTC on 11 July 2013.

S-3 Flight maps of in-situ profiles

The following figures show the Falcon position during the measurements considered for Fig. 9.

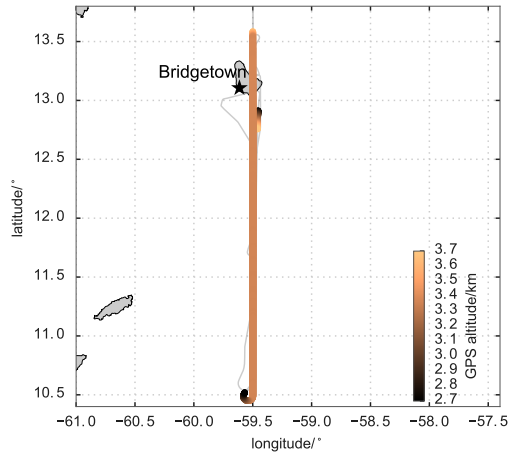

Figure S-3: Flight position during measurements shown in Fig. 9 for 22 June 2013

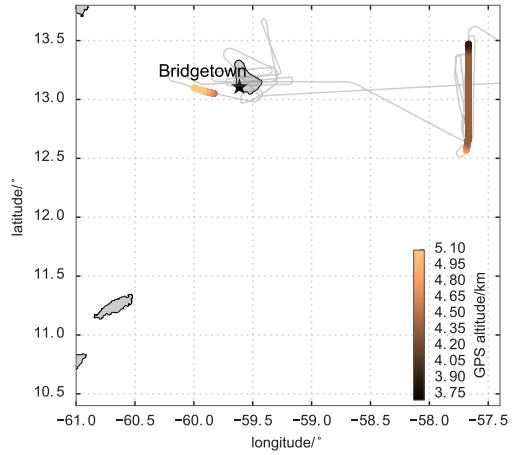

Figure S-4: Flight position during measurements shown in Fig. 9 for 10 July 2013

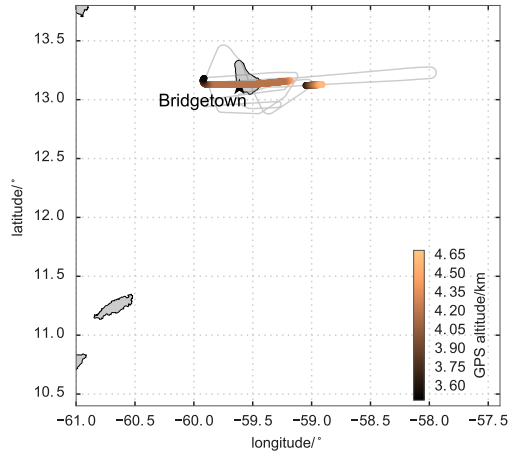

Figure S-5: Flight position during measurements shown in Fig. 9 for 11 July 2013

S-4 Additional CALIOP data analysis

In Section 5.1 of the paper we describe how we selected the profiles for averaging over five years. The averaged profiles are shown in Fig. 10. In this supplement we present some further aspects of the CALIOP data used.

S-4.1 Geographic location of selected profiles

Fig. S-6 shows the region where the selected CALIOP profiles were measured. The different colors denote the different averaging regions (same colors as in Fig. 10). The area of the circles is proportional to the number of selected profiles (for Fig. 10) grouped within 5°x5° regions.

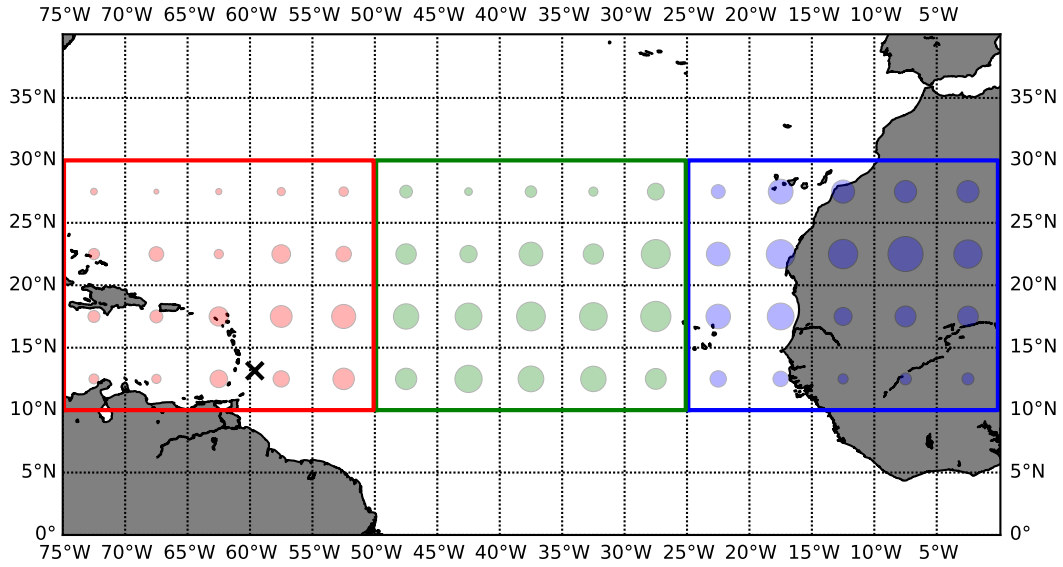

Figure S-6: Geographic region of CALIOP study with circle areas proportional to the number of selected profiles within 5°x5° regions. 'x' denotes Barbados.

S-4.2 Year to year variability

We investigate the year to year variability of the average δ_l profile. The Figs. S-7 to S-11 are analogous to Fig. 10 of the paper, but for individual years from 2007 to 2011.

Comparison of the profiles of the individual years shows some variability between the years, but in general the height dependence of δ_l is very similar each year. The variability between the years is in most cases smaller than the statistical uncertainty of the averaged δ_l.

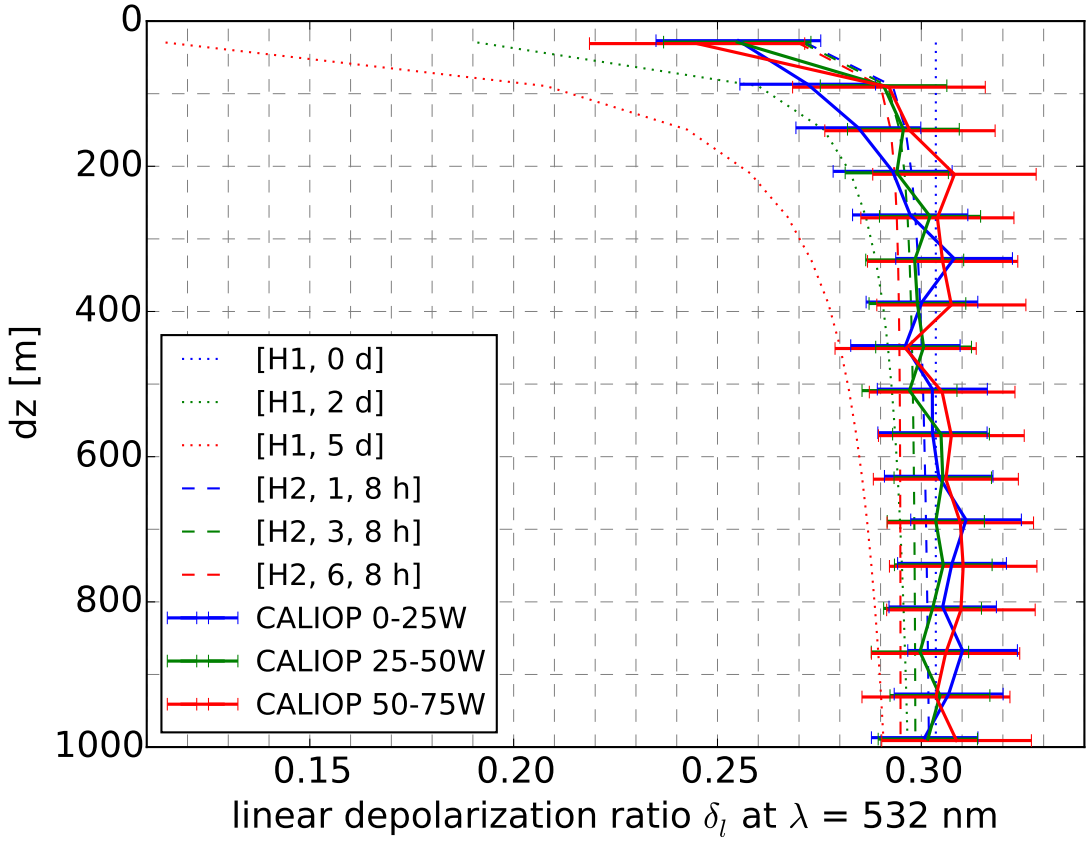

Figure S-7: Average δ_l profile for summer 2007. For the different regions, 2328 / 2840 / 1212 profiles were averaged.

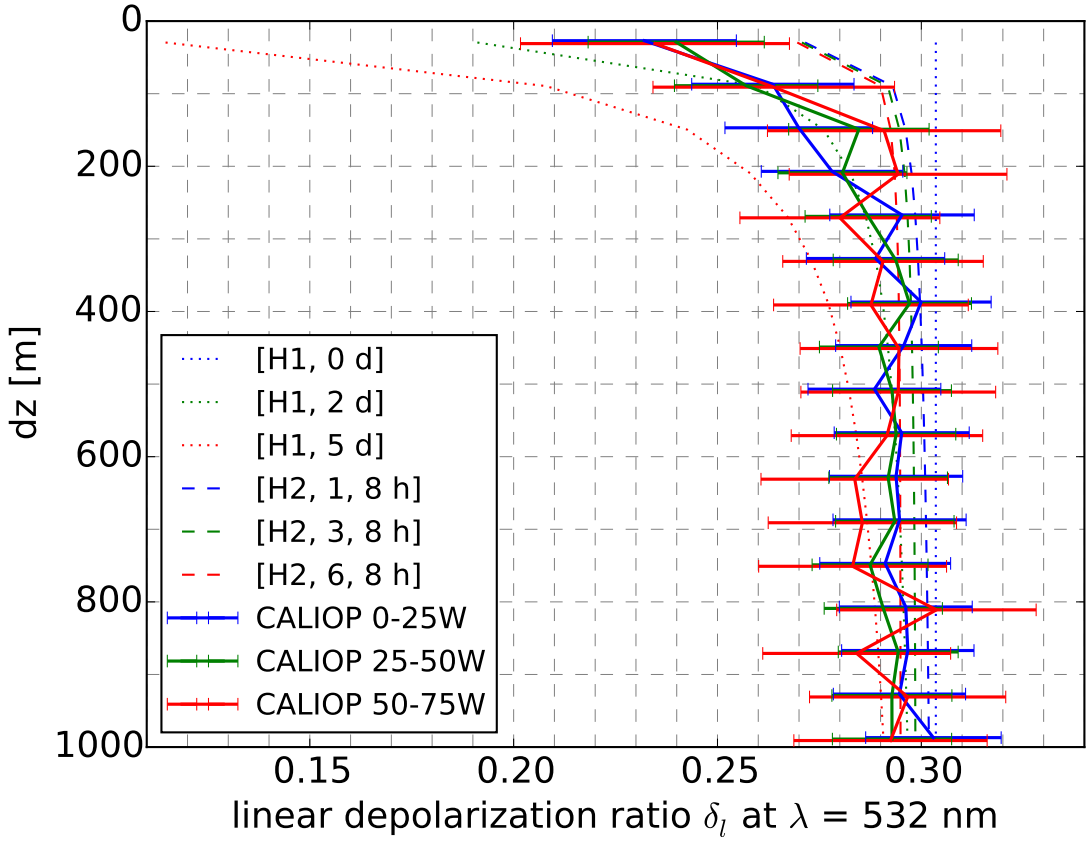

Figure S-8: Average δ_l profile for summer 2008. For the different regions, 1624 / 1892 / 831 profiles were averaged.

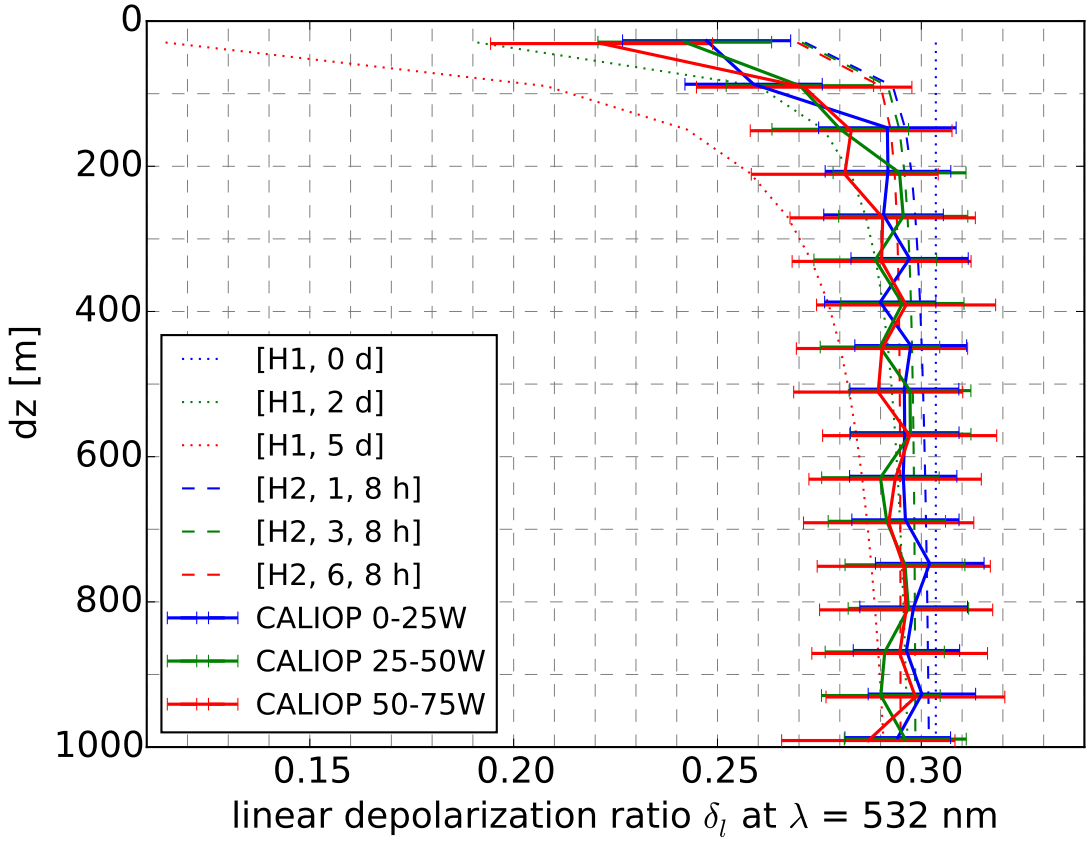

Figure S-9: Average δ_l profile for summer 2009. For the different regions, 2066 / 1708 / 917 profiles were averaged.

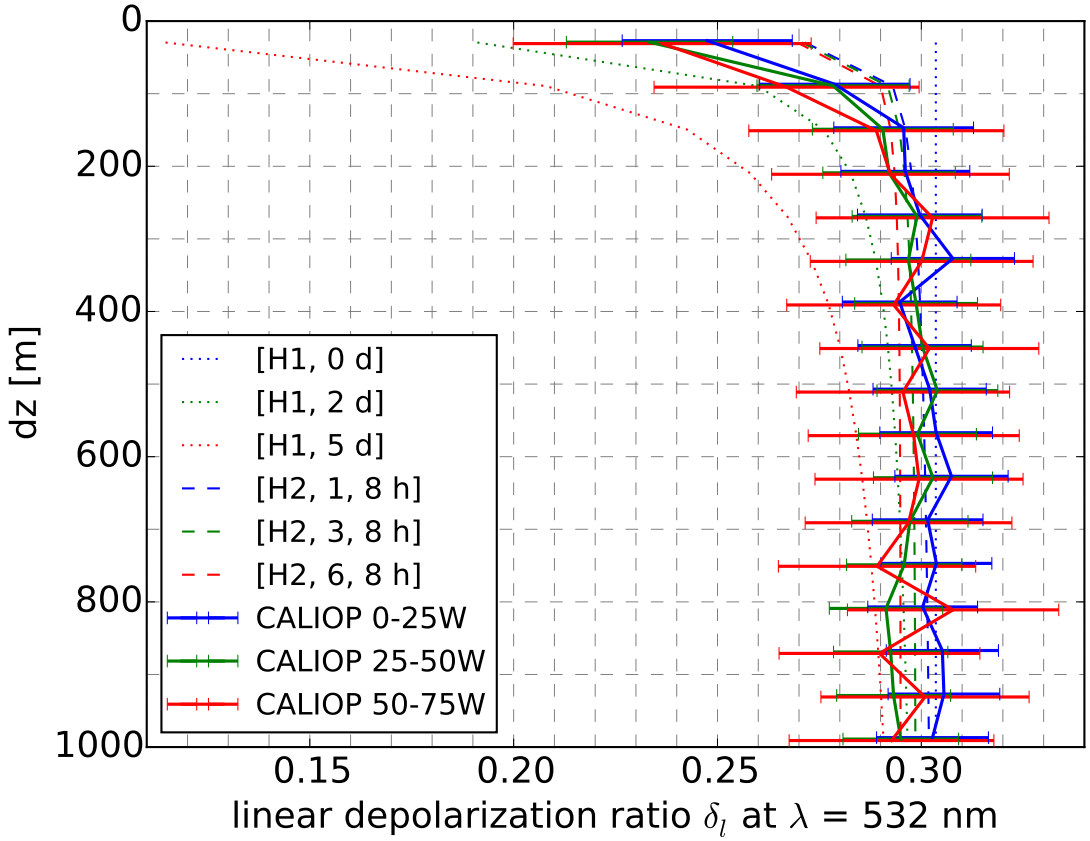

Figure S-10: Average δ_l profile for summer 2010. For the different regions, 2041 / 1844 / 646 profiles were averaged.

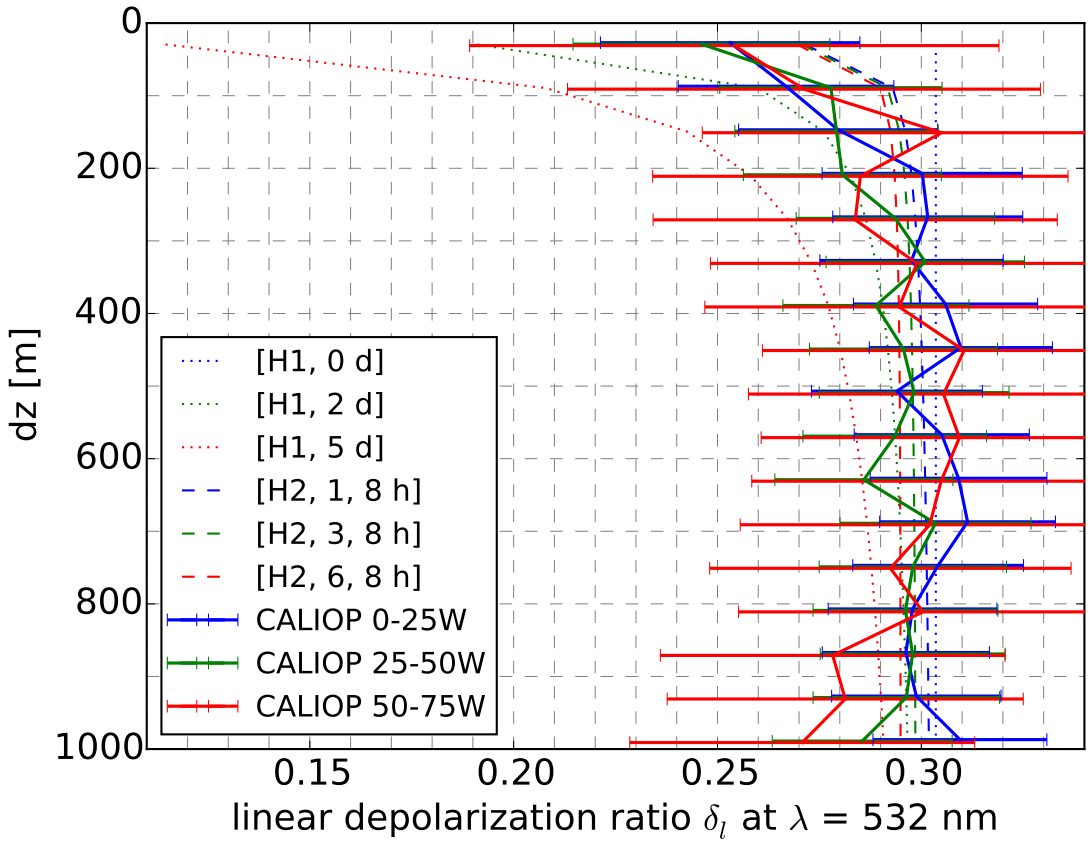

Figure S-11: Average δ_l profile for summer 2011. For the different regions, 1002 / 830 / 240 profiles were averaged.

S-4.3 No aerosol in uppermost sub-bin

The following Fig. S-12 is analogous to Fig. 10 of the paper, but considers only profiles where the upper sub-bin (30m) of the uppermost aerosol-containing bin was classified as aerosol-free (not as aerosol-containing like in Fig. 10).

Comparison of Fig. S-12 with Fig. 10 shows a difference in the second bin from the top, which is shifted to smaller δ_l in case the uppermost sub-bin is aerosol-free. However, if dz in Fig. S-12 is corrected for the uppermost sub-bin being above the SAL, i.e. dz is reduced by 30 m, the values of the second bin in Fig. S-12 are consistent with Fig. 10, i.e. the values of 0.25-0.26 are almost the same as the average between first and second bin in Fig. 10. δ_l in the upper bin of Fig. S-12 is increased compared to what one would expect from the shape of the profile below. This deviation might be due to some artefact in the data evaluation procedures, but as the amount of aerosol is low in this bin, the statistical uncertainties are large.

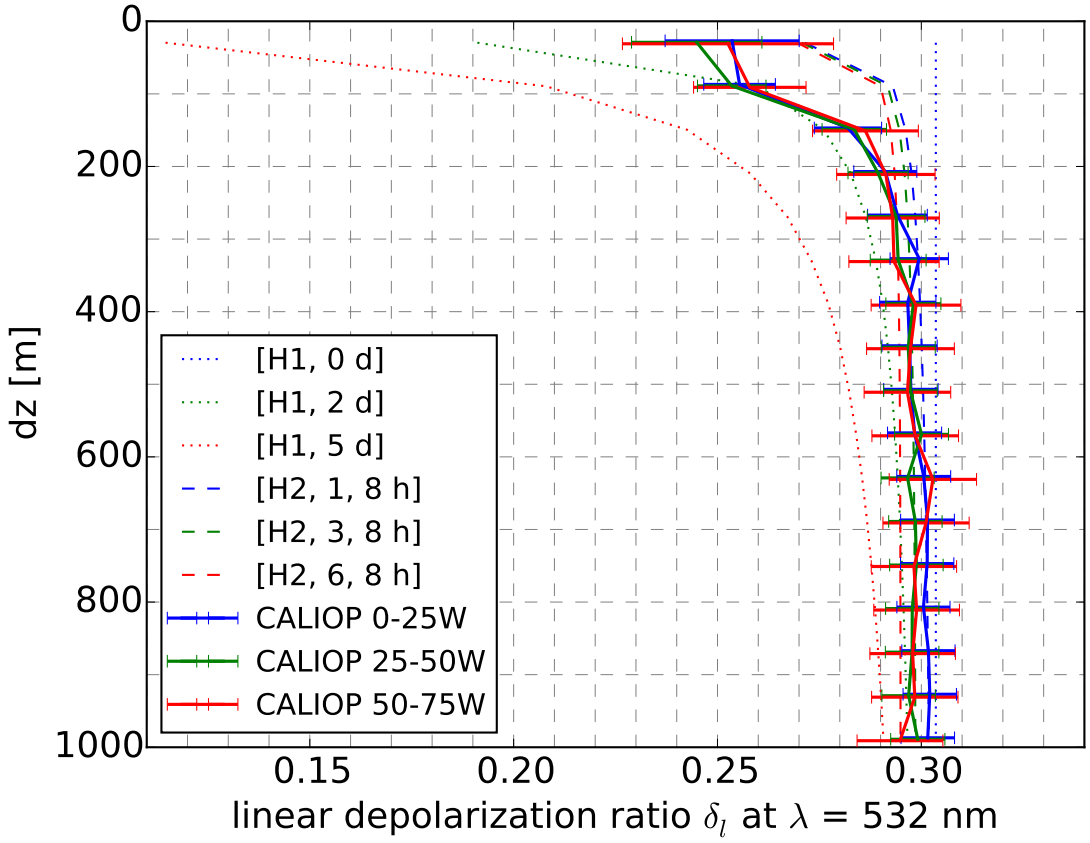

Figure S-12: Average δ_l profile considering only profiles without aerosol in uppermost sub-bin. For the different regions, 9342 / 9158 / 3784 profiles were averaged.

S-4.4 Horizonal averaging

The following Fig. S-13 is analogous to Fig. 10 of the paper, but considers also profiles which were horizontally averaged over 20 and 80 km.

Comparison with Fig. 10 shows that the averaged profiles are the same within their statistical uncertainty, indicating that the averaged profiles are insensitive to the selection of horizontal averaging range. The statistical uncertainty in Fig. S-13 is lower than in Fig. 10 because of the higher number of profiles considered for Fig. S-13.

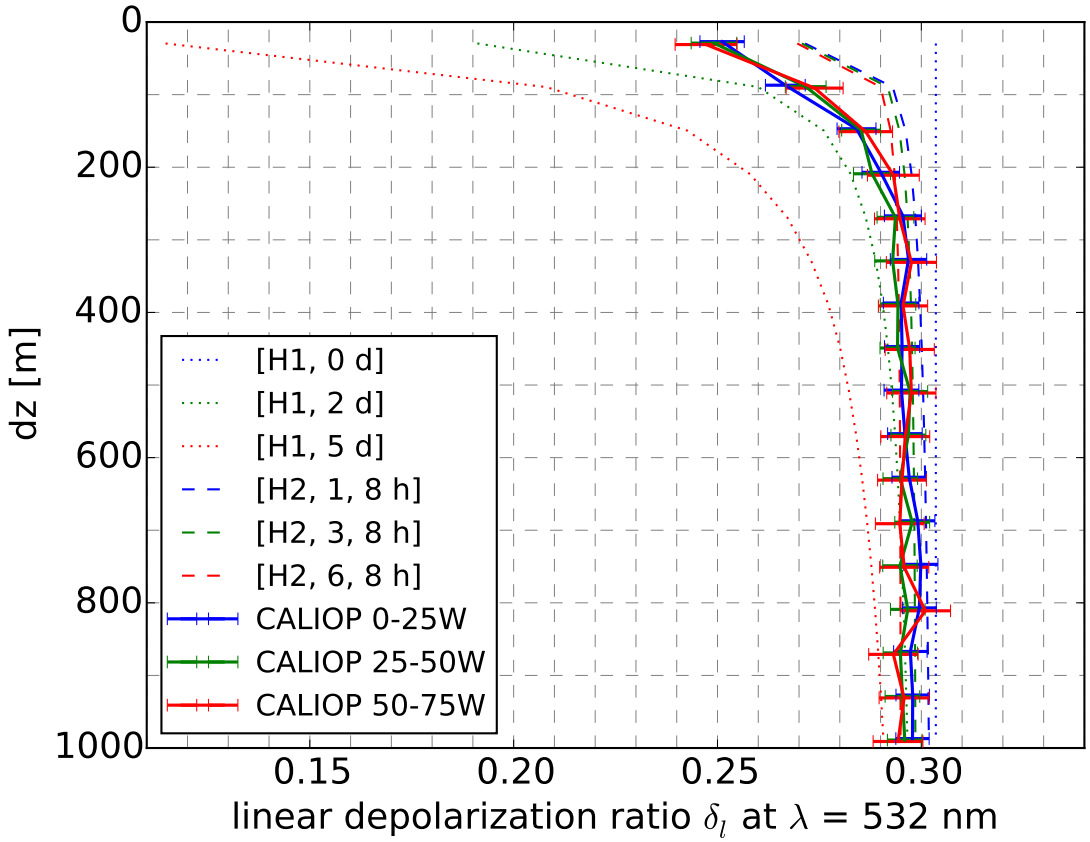

Figure S-13: Average δ_l profile considering profiles horizontally averaged over 5, 20, 80 km. For the different regions, 31106 / 28312 / 14506 profiles were averaged.

S-4.5 Linear depolarization ratio threshold

The following Fig. S-14 is analogous to Fig. 10 of the paper, but without requiring the linear depolarization ratio, averaged over 17 uppermost aerosol-containing bins, to be larger than 0.1.

Comparison with Fig. 10 reveals that the linear depolarization ratio threshold has almost no effect on the averaged profiles. Only very few profiles (9 / 4 / 20 in the different regions) are sorted out by the linear depolarization ratio threshold criterion in case of Fig. 10, indicating that no significant amounts of non-Saharan aerosol occurs in the investigated region and height range during summer.

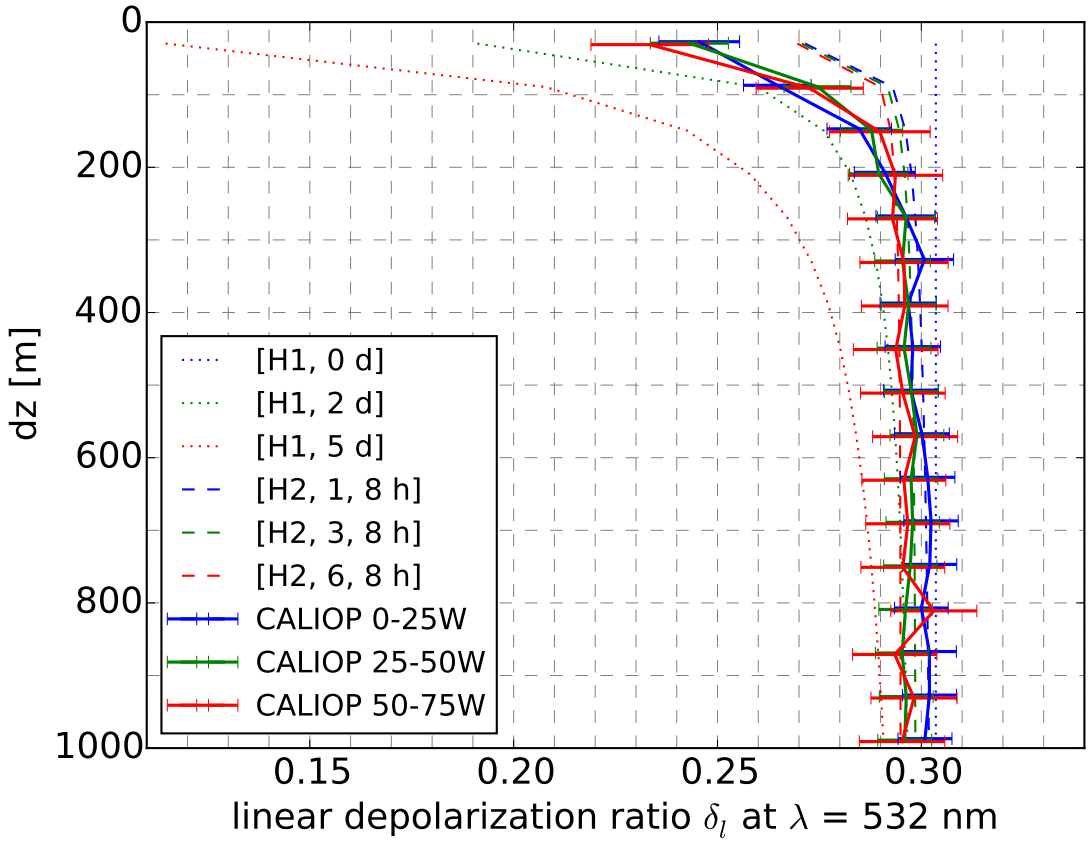

Figure S-14: Average δ_l profile without using the average linear depolarization ratio as a profile selection criterion. For the different regions, 9070 / 9118 / 3866 profiles were averaged.

S-4.6 Cloud-aerosol discrimination (CAD) score

The following Fig. S-15 is analogous to Fig. 10 of the paper, but considers only profiles in which all bins have a cloud-aerosol discrimination (CAD) score of -100. The CAD score provides the confidence level for the discrimination between aerosol and cloud in the CALIOP data evalulation. A CAD score value of -100 means that the bin is classified as aerosol-containing with complete confidence. +100 means complete confidence for classification as cloud-containing. The CAD score of the profiles considered in Fig.10 of the paper varies in the range from -100 to 0.

Comparison of Fig. S-15 with Fig. 10 reveals that using only profiles with complete confidence slightly reduces the average δ_l values, but it does not change the overall shape of the profiles.

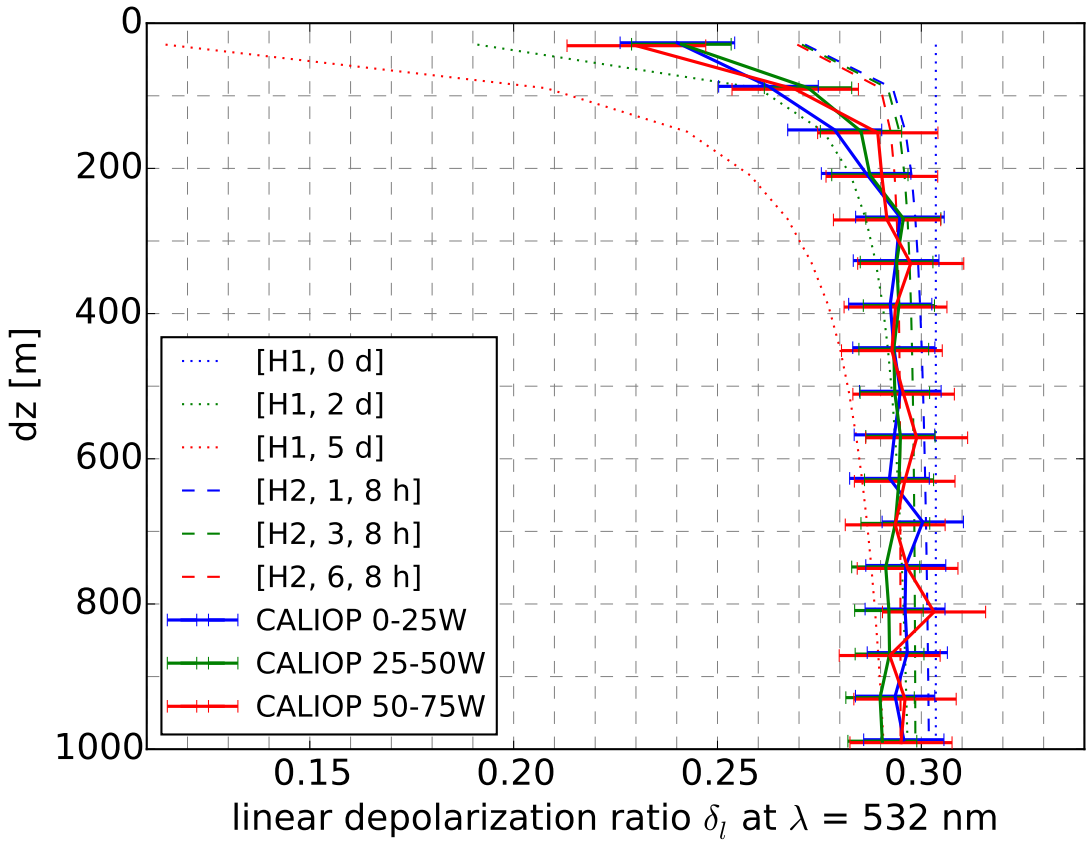

Figure S-15: Average δ_l profile considering only profiles with CAD score equal to -100 within the upper 1 km of the SAL. For the different regions, 4461 / 5616 / 2736 profiles were averaged.

S-4.7 Average backscatter coefficient

The following Fig. S-16 shows the average backscatter coefficient β at $\lambda = 532$ nm of the profiles considered in Fig. 10 of the paper together with modeled β-profiles for comparison. The amount of particles in the model is scaled such that β in the lowermost bin at $t_s = 0$ matches with the measurements near the source (blue solid line). The error bars show the statistical uncertainty of the average.

The figure reveals that the average backscatter coefficient in the selected profiles is similar in the different regions (see solid lines) while we would expect significant changes of the β-profile with transport time/region in case of H1 (see dotted lines). The backscatter coefficient in the uppermost bin is on average about one third of the backscatter coefficient in about 1 km below SAL top. The measured average β profile is not well captured by both models.

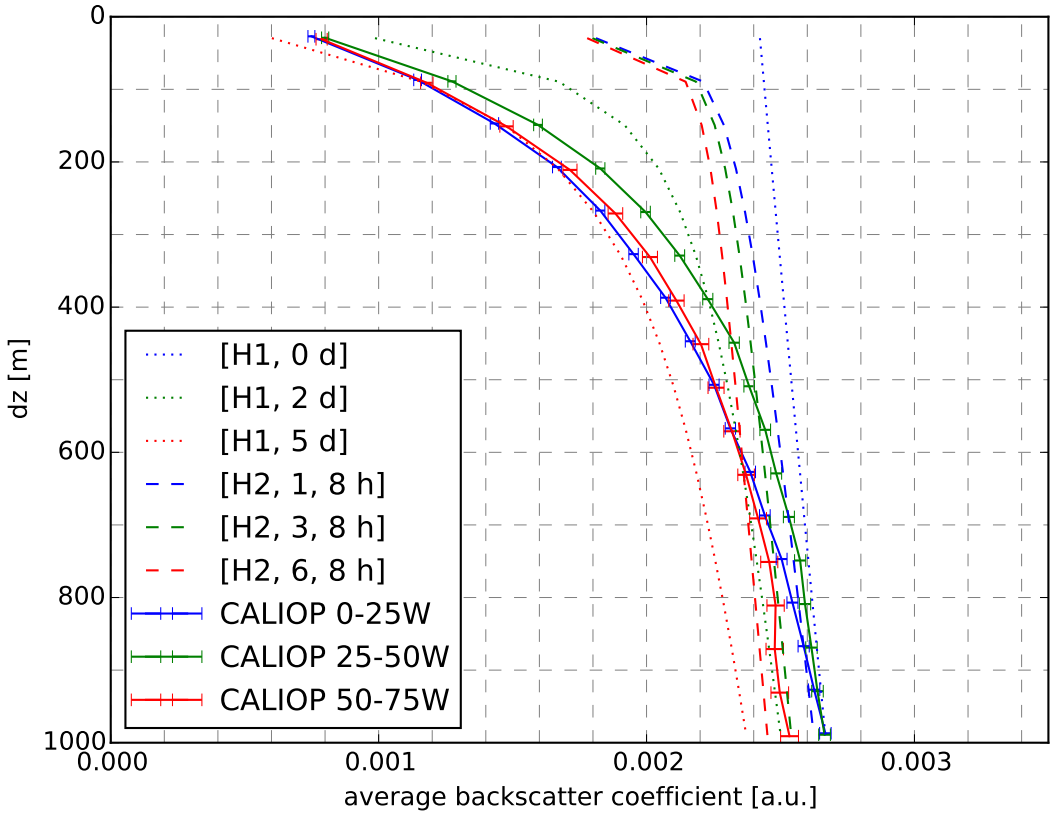

Figure S-16: Average backscatter coefficient β with the estimated statistical uncertainty of the average (solid lines). For comparison, different model profiles are shown.

S-4.8 Statistics over profiles used for averaging

The following figures show histograms over all profiles used in Fig. 10 of the paper, first a histogram of the SAL top height and second a histogram of the δ_l averaged over the upper 17 bins of each profile.

The SAL top height histogram (Fig. S-17) shows on average a decrease of the SAL top height with increasing transport distance. For 0-25W, most SAL top heights are between 4.5 km and 6.5 km, for 25-50W most tops are between 4.0 km and 6.0 km, and for 50-75W most SAL tops are between 3.0 km and 5.5 km.

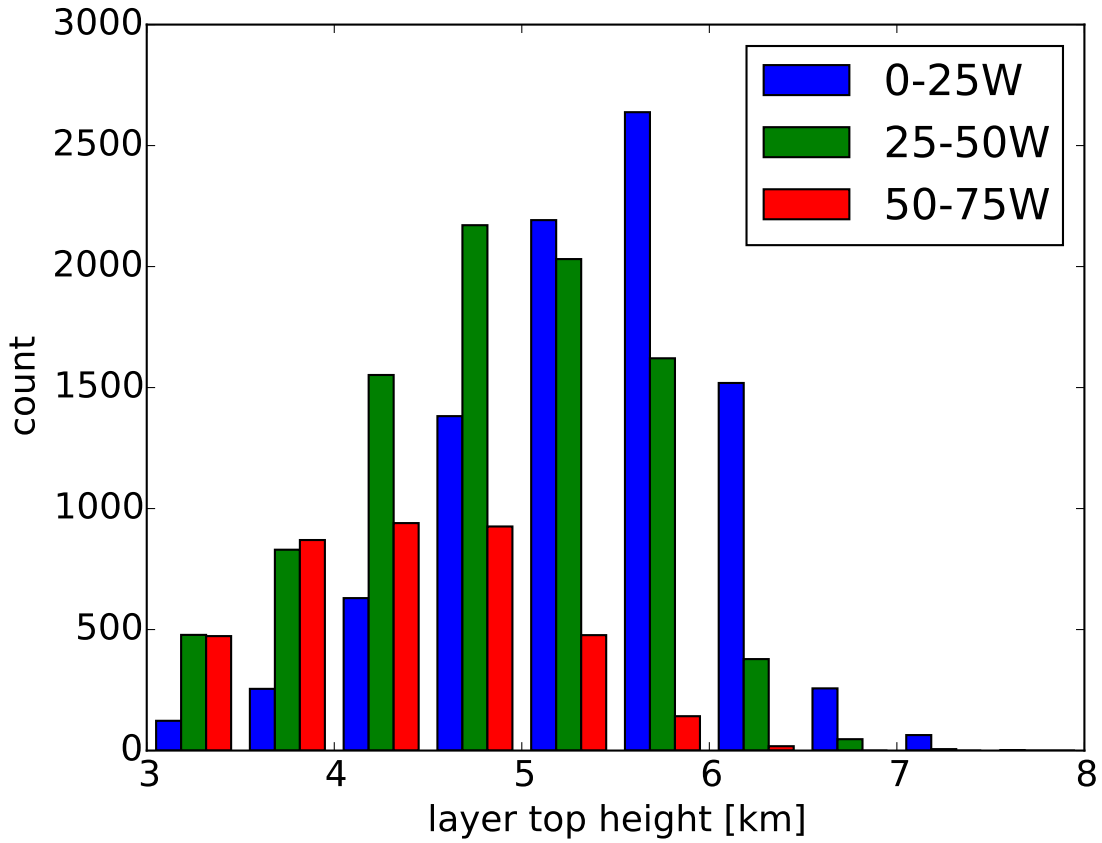

Figure S-17: Histogram of SAL top height.

The δ_l histograms (Fig. S-18) peaks at slightly below 0.3 and only very few layer-averaged δ_l values are smaller than 0.15 or larger than 0.45. The shapes of the histograms are almost the same for each region. We did not investigate if the width of histograms can be explained by the statistical uncertainty of the layer-averaged δ_l alone or to which extend it reflects also a natural variability of δ_l. This could be a topic for future research.

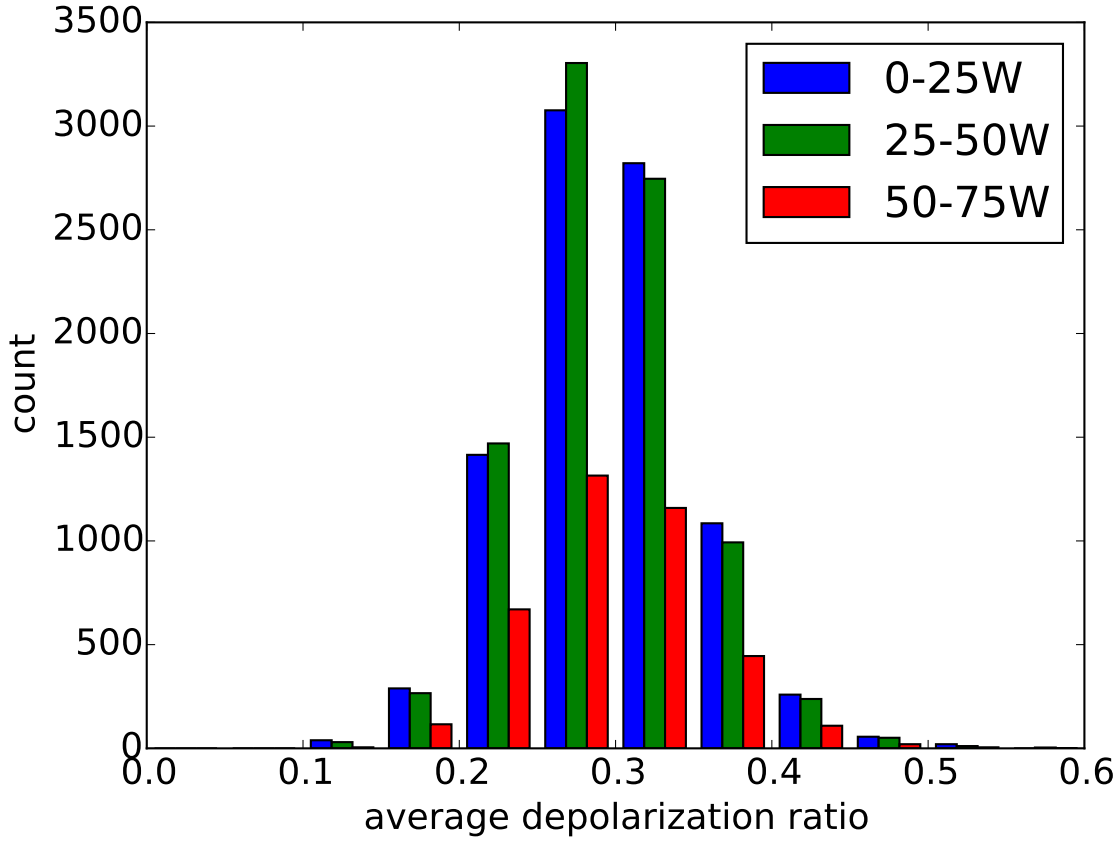

Figure S-18: Histogram of layer-averaged linear depolarization ratio.